Inorg. Chem. **2008**, *47*, 5314−5323

Redox Transformations of Bis(2,2′-bipyridine)(1-methyl-1-pyridin-2-yl-ethylamine)ruthenium(II)

Justin Neill,[†] Anna S. Nam, Kevin M. Barley, Benjamin Meza,[‡] and David N. Blauch*

Department of Chemistry, Davidson College, Davidson, North Carolina 28035

Received March 17, 2008

The amineruthenium(II) complex $Ru(bpy)_2(mpea)^{2+}$ has been prepared by the direct reaction of 1-methyl-1-pyridin-2-yl-ethylamine (mpea) with $Ru(bpy)_2Cl_2$ in ethanol/water and isolated as the hexafluorophosphate salt. Electrochemical analysis of this complex shows that it undergoes sequential one-electron oxidations to an amidoruthenium(III) intermediate ($E^{\circ\prime} = 1.086$ V vs NHE) and then to an amidoruthenium(IV) ($E^{\circ\prime} = 0.928$ V) or imidoruthenium(IV) ($E^{\circ\prime} = 1.083$ V) complex, depending upon the solution pH ($pK_a = 2.62$ for the amidoruthenium(IV) species). At higher potentials ($E_{pa} = 1.5$ V in 1.0 M H_2SO_4), the amido- or imidoruthenium(IV) species is irreversibly oxidized to the corresponding nitrosoruthenium(II) complex. The mechanism for this transformation appears, on the basis of b3lyp/cpcm/cep-31g(d) computations, to proceed through an imidoruthenium(V) intermediate, which is rapidly attacked by water to yield a Ru(II)-bound hydroxylamine radical, which is readily oxidized and deprotonated to produce the nitrosoruthenium(II) complex. The nitrosoruthenium(II) complex is quantitatively reduced to the original $[Ru(bpy)_2(mpea)]^{2+}$ complex at relatively negative potentials ($E_{pc} = -0.2$ V in 1.0 M H_2SO_4).

Introduction

Recent investigations in our laboratory have examined the catalytic role of ruthenium in oxidative transformations of coordinated amines, with particular interest in the reactivity of high oxidation state amido- and imido- intermediates.[1] In almost all cases, oxidation of an amineruthenium(II) complex leads to dehydrogenation of the ligand, yielding a coordinated imine.[2–4] For some primary amines, further oxidation of the imine to a nitrile is also possible.[3a] The utilization of ruthenium complexes as catalysts for the synthesis of imines and nitriles has also been described.[5] Mechanistic studies of oxidative dehydrogenation in amineruthenium(II) systems have proposed amidoruthenium(III)[6] and amidoruthenium(IV)[7,8] species as reactive intermediates. Our strategy has been to employ ligands possessing structural constraints designed to inhibit the final imine-forming step. With the preferred imine-forming pathway blocked, the highly oxidized intermediate may be sufficiently long-lived to permit detailed study.

A key requirement for imine formation is the presence of a hydrogen α to the amine nitrogen. With the metal in an oxidized state, deprotonation of the α-hydrogen leads to a 1,3-reductive elimination for a broad range of complexes owing to π electron delocalization across the C−N−metal linkage.[9] In this study, we have chosen a well-studied amine

* To whom correspondence should be addressed. E-mail: dablauch@davidson.edu. Fax: 704-894-2709.

† Present address: University of Virginia, Charlottesville, Virginia, 22904.

‡ Present address: Virginia Commonwealth University, Richmond, Virginia, 23284.

(1) Chang, J.; Plummer, S.; Berman, E. S. F.; Striplin, D.; Blauch, D. *Inorg. Chem.* **2004**, *43*, 1735–1742.

(2) (a) Lane, B. C.; Lester, J. E.; Basolo, F. *J. Chem. Soc., Chem. Commun.* **1971**, 1618–1619. (b) Mahoney, D. F.; Beattie, J. K. *Inorg. Chem.* **1973**, *12*, 2561–2565. (c) Alvarez, V. E.; Allen, R. J.; Matsubara, T.; Ford, P. C. *J. Am. Chem. Soc.* **1974**, *96*, 7686–7692. (d) Diamond, S. E.; Tom, G. M.; Taube, H. *J. Am. Chem. Soc.* **1975**, *97*, 2661–2664.

(3) (a) Keene, F. R.; Salmon, D. J.; Meyer, T. J. *J. Am. Chem. Soc.* **1976**, *98*, 1884–1889. (b) Brown, G. M.; Weaver, T. R.; Keene, F. R.; Meyer, T. J. *Inorg. Chem.* **1976**, *15*, 190–196. (c) Whebell, G. W.; Keene, F. R. *Aust. J. Chem.* **1986**, *39*, 2027–2035.

(4) (a) Yamaguchi, M.; Yamagishi, T. *Inorg. Chem.* **1993**, *32*, 2981–2982. (b) Yamaguchi, M.; Machiguchi, K.; Mori, T.; Kikuchi, K.; Ikemoto, I.; Yamagishi, T. *Inorg. Chem.* **1996**, *35*, 143–148.

(5) (a) Murahashi, S.-I.; Naota, T.; Hiroshi, T. *J. Chem. Soc., Chem. Commun.* **1985**, 613–614. (b) Bailey, A. J.; James, B. R. *Chem. Commun.* **1996**, 2343–2344.

(6) Toma, H. E.; Tsurumaki, M. *J. Braz. Chem. Soc.* **1990**, *1*, 17–21.

(7) (a) Bernhard, P.; Sargeson, A. M.; Anson, F. C. *Inorg. Chem.* **1988**, *27*, 2754–2760. (b) Bernhard, P.; Sargeson, A. M. *J. Am. Chem. Soc.* **1989**, *111*, 597–606. (c) Bernhard, P.; Anson, F. C. *Inorg. Chem.* **1989**, *28*, 3272–3274. (d) Bernhard, P.; Bull, D. J.; Bürgi, H.-B.; Osvath, P.; Raselli, A.; Sargeson, A. M. *Inorg. Chem.* **1997**, *36*, 2804–2815.

(8) (a) Ridd, M. J.; Keene, F. R. *J. Am. Chem. Soc.* **1981**, *103*, 5733–5740. (b) Keene, F. R.; Ridd, M. J.; Snow, M. R. *J. Am. Chem. Soc.* **1983**, *105*, 7075–7081.

(9) Collins, T. J. *Acc. Chem. Res.* **1994**, *27*, 279–285.

10.1021/ic800483g CCC: $40.75
Published on Web 05/07/2008

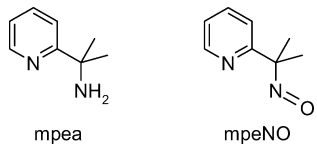

Figure 1. Structures of mpea and mpeNO ligands.

ligand, 2-aminomethylpyridine (ampy), and introduced methyl groups in the α positions to obtain 1-methyl-1-pyridin-2-yl-ethylamine (mpea), as shown in Figure 1. Oxidation of Ru(bpy)$_2$(ampy)$^{2+}$ results in the quantitative conversion of 2-aminomethylpyridine to the corresponding imine.[8] By contrast, Ru(bpy)$_2$(mpea)$^{2+}$ may be reversibly oxidized to yield amidoruthenium(III), amidoruthenium(IV), and imidoruthenium(IV) species, whose electrochemical and spectroscopic properties are described in this report. Further oxidation produces a nitrosoruthenium(II) complex, which may be reduced to the original Ru(bpy)$_2$(mpea)$^{2+}$ complex.

Experimental Section

General. Water was distilled and deionized prior to use. Anhydrous THF was obtained from Aldrich. All other solvents and reagents were of analytical grade and were used without additional purification. Methyllithium (1.6 M in ether) was standardized by titration with *sec*-butanol. Elemental analyzes were performed by Quantitative Technologies Inc.

1-Methyl-1-pyridin-2-yl-ethylamine (mpea). The mpea ligand was prepared by the addition of CH_3CeCl_2 to 2-cyanopyridine following the general approach of Ciganek.[10] The CH_3CeCl_2 was prepared from $CeCl_3 \cdot 7H_2O$ (40.2 g, 0.11 mol), according to a published procedure.[11] A solution of 2-cyanopyridine (11.2 g, 0.11 mol) in THF was added to a dispersion of CH_3CeCl_2 in THF at −78 °C over a period of 20 min. After stirring for 2 h, concentrated aqueous ammonia (75 mL) was added, and the mixture was warmed to room temperature. The brown residue was removed by filtration with Celite, and the filtrate was extracted with CH_2Cl_2 (3 × 50 mL). The organic solution was dried over Na_2SO_4, and the solvent was removed by rotary evaporation. The residue was dissolved in aqueous HCl, and the pH was adjusted to 6.8 by the addition of solid Na_2CO_3. This solution was washed with CH_2Cl_2, made strongly alkaline by the addition of 50% NaOH, and extracted with CH_2Cl_2 (4 × 40 mL). The organic solution was dried over Na_2SO_4, and the solvent was removed by rotary evaporation. The residue was vacuum distilled (32−34 °C at 1−2 torr) to yield 4.0 g (53%) of a colorless liquid. ^{1}H NMR (400 MHz, $CDCl_3$): δ 1.51 (s, 6 H, C*H*$_3$), 1.98 (br s, 2 H, N*H*$_2$), 7.13 (dd, J = 4.8 and 7.4 Hz, 1 H, pyridyl H5), 7.46 (d, J = 8.0 Hz, 1 H, pyridyl H3), 7.64 (dd, J = 7.4 and 8.0 Hz, 1 H, pyridyl H4), 8.56 (d, J = 4.8 Hz, 1 H, pyridyl H6). MS (CI): *m*/*z* calcd for $C_8H_{13}N_2$ [M + H]$^+$, 137; found, 137. In some of our preparations, as an alternative to the vacuum distillation, the mpea was isolated as the hydrochloride salt by dissolving the crude free ligand in concentrated HCl and removing the water by heating under reflux with toluene through a Dean−Stark trap. Ether was added to the toluene solution, and the white solid was isolated by filtration, recrystallized from *sec*-butanol, and dried under vacuum. ^{1}H NMR (400 MHz, D_2O): δ 1.73 (s, 6 H, C*H*$_3$), 7.42 (dd, J = 4.9 and 7.7 Hz, 1 H, pyridyl H5), 7.58 (d, J = 8.1 Hz, 1 H, pyridyl H3), 7.92 (dd, J = 7.7 and 8.1 Hz, 1 H, pyridyl H4), 8.56 (d, J = 4.9 Hz, 1 H, pyridyl H6).

[Ru^{II}(bpy)$_2$(mpea)](PF$_6$)$_2$. A solution of mpea·HCl (0.931 g, 5.39 mmol) and Na_2CO_3 (0.588 g, 5.55 mmol) in water (20 mL) was added to a solution of Ru(bpy)$_2$Cl$_2$ (2.34 g, 4.51 mmol) in ethanol (50 mL) under nitrogen. The resulting solution was heated under reflux under nitrogen for 4 h, after which NH_4PF_6 (8.03 g, 49.3 mmol) was added and the mixture was cooled overnight in a refrigerator. The product was isolated by filtration, recrystallized from an ethanol/water mixture, and dried under vacuum, yielding 2.98 g (79%) of dark red microcrystals. Anal. Calcd for $C_{28}H_{28}F_{12}N_6P_2Ru$: C, 40.06%; H, 3.36%; N, 10.01%. Found: C, 40.16%; H, 3.26%; N, 9.82%. ^{1}H NMR data is available in the Supporting Information. MS (ESI): *m*/*z* calcd for $C_{28}H_{28}N_6Ru$ M^{2+}, 275.1; found, 275.1.

[Ru^{II}(bpy)$_2$(mpeNO)](PF$_6$)$_2$. A solution of [Ru^{II}(bpy)$_2$(mpea)](PF$_6$)$_2$ (54 mg, 64 μmol) in a pH 4.0 acetate buffer (61 mL) was exhaustively electrolyzed at +1.40 V versus Ag/AgCl at a cylindrical RVC working electrode (q = 23.4 C, n = 3.8). The electrolyzed solution was treated with NH_4PF_6 (3.33 g, 20.4 mmol) and cooled in a refrigerator overnight. The residue was collected by vacuum filtration, washed with cold water (3 × 3 mL), and dried under vacuum to yield 46 mg (84%) of an olive green powder. Anal. Calcd for $C_{28}H_{26}F_{12}N_6OP_2Ru$: C, 39.40%; H, 3.07%; N, 9.85%. Found: C, 39.18%; H, 2.81%; N, 9.66%. ^{1}H NMR data is available in the Supporting Information. MS (ESI): *m*/*z* calcd for $C_{28}H_{26}N_6ORu$ M^{2+}, 282.1; found, 282.1.

Spectroscopy. ^{1}H, COSY, and *J*-resolved NMR spectroscopy were performed on a Jeol Eclipse spectrometer (400 MHz). Chemical shifts are reported in parts per million and referenced to TMS. UV−vis spectroscopy was performed on an HP 8453 diode-array spectrometer. Solvatochromatic studies employed DMSO, DMF, THF, methanol, acetone, CH_2Cl_2, 1,2-dichloroethane, and water as solvents. Mass spectrometry was performed by the Mass Spectrometry Laboratory in the Department of Chemistry and Biochemistry at the University of South Carolina.

Electrochemistry. Cyclic voltammetry was performed with a PAR 273A potentiostat using a single-compartment cell equipped with a glassy carbon disk working electrode (0.0707 cm^2) and a platinum counter electrode. Potentials were recorded versus a Ag/AgCl reference electrode but are reported versus NHE. Formal potentials are reported for 1 M H$^+$. Measurements were obtained at 21 ± 1 °C, and all solutions were purged with nitrogen prior to analysis. Coulometry was performed using 40−70 mL of solution and a cylindrical RVC working electrode (Bioanalytical Systems MF-2077). Spectroelectrochemical data was obtained by performing a bulk electrolysis at the chosen potential and then drawing a 0.3 mL sample for UV−vis analysis.

Computations. Density functional theory (DFT) computations employing Becke's three-parameter hybrid functional[12] using the Lee, Yang, and Parr correlation function[13] (b3lyp) were performed using the Gaussian 03 software package.[14] The split-valence ecp basis set of Stevens, Basch, Krauss, and Jasien with polarization functions on the second-row nonmetals, cep-31g(d), was used for all computations.[15] Wave function stability calculations were performed to confirm that ground-state wave functions had been

(10) Ciganek, E. *J. Org. Chem.* **1992**, *57*, 4521–4527.
(11) Takeda, N.; Imamoto, T. *Org. Synth.* **2004**, 200.
(12) (a) Becke, A. D. *Phys. Rev. A* **1988**, *38*, 3098–3100. (b) Becke, A. D. *J. Chem. Phys.* **1993**, *98*, 1372–1377. (c) Becke, A. D. *J. Chem. Phys.* **1993**, *98*, 5648–5652. (d) Stevens, P. J.; Devlin, F. J.; Chablowski, C. F.; Frisch, M. J. *J. Phys. Chem.* **1994**, *98*, 11623–11627.
(13) Lee, C.; Yang, W.; Parr, R. G. *Phys. Rev. B* **1988**, *37*, 785–789.
(14) Fisch, M. J.; et al. *Gaussian 03*, revision D.01; Gaussian, Inc.: Wallingford, CT, 2004.
(15) (a) Stevens, W.; Basch, H.; Krauss, J. *J. Chem. Phys.* **1984**, *81*, 6026–6033. (b) Stevens, W. J.; Krauss, M.; Basch, H.; Jasien, P. G. *Can. J. Chem.* **1992**, *70*, 612–630. (c) Cundari, T. R.; Stevens, W. J. *J. Chem. Phys.* **1993**, *98*, 5555–5565.

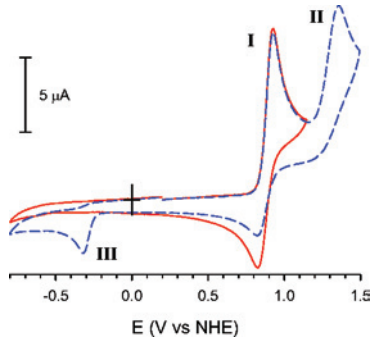

Figure 2. Cyclic voltammograms (25 mV s^{-1}) of 0.82 mM $Ru(bpy)_2(mpea)^{2+}$ in aqueous acetate buffer (pH 4.07). Voltammetric wave **III** is only observed after sweeping through wave **II**.

obtained. Frequency computations provided standard thermochemical properties (298 K) and verified that each optimized geometry corresponded with an energy minimum (no imaginary frequencies). Energies and oscillator strengths for electronic transitions were obtained using nonequilibrium time-dependent density functional theory (TD-DFT)[16] with gas-phase geometries that include one or two water molecules at the amine, amide, imide, or nitroso sites. The electronic spectrum was modeled as the sum of Gaussian band shapes associated with each transition assuming a full width at half-maximum (fwhm) of 3000 cm^{-1}.[17] As other researchers have observed, the energies for the calculated absorbance maxima are systematically higher than the experimental values.[18] In order to clearly examine trends in the results, we have shifted all calculated transition energies by −0.13 eV to make the calculated λ_{max} for the most intense $Ru(bpy)_2(mpea)^{2+}$ band coincide with the experimental value of 289 nm. The free energies of solvation were obtained using Barone and Cossi's implementation of the conductor-like polarizable continuum model (cpcm)[19] with a dielectric constant of 78.36 (water) and the uahf radii using the gas-phase geometries, and the values were corrected to coincide with a gas-phase standard state of 1 atm and an aqueous standard state of 1 mol L^{-1}.[20] Tissandier's value of −264.0 kcal mol^{-1} for the standard free energy of solvation for the proton was used.[21]

Results

Electrochemistry. Cyclic voltammetry of $[Ru(bpy)_2(mpea)]^{2+}$ in aqueous solution revealed three voltammetric waves, as depicted in Figure 2. The first wave (**I**) is a two-electron process (coulometry gives $n = 1.9$) that is quasireversible at low pH ($\Delta E_p = 34$ mV at 9 mV s^{-1} in 1.0 M H_2SO_4) and becomes increasingly less reversible as the pH increases (Figure 3). The product from the oxidation associated with wave **II** is reduced at wave **III**, which is present only after scanning through wave **II**. Exhaustive electrolysis at potentials beyond wave **II** yielded the nitrosoruthenium(II) complex $[Ru(bpy)_2(mpeNO)]^{2+}$ (Figure 1), which corresponds with a net four-electron, four-proton oxidation of $Ru(bpy)_2(mpea)^{2+}$ (coulometry gives $n = 3.8$). Correspondingly, exhaustive electrolysis of $[Ru(bpy)_2(mpeNO)]^{2+}$ at potentials in wave **III** led to the quantitative recovery of the original $[Ru(bpy)_2(mpea)]^{2+}$ complex, as verified by ^1H NMR and UV−vis spectroscopy.

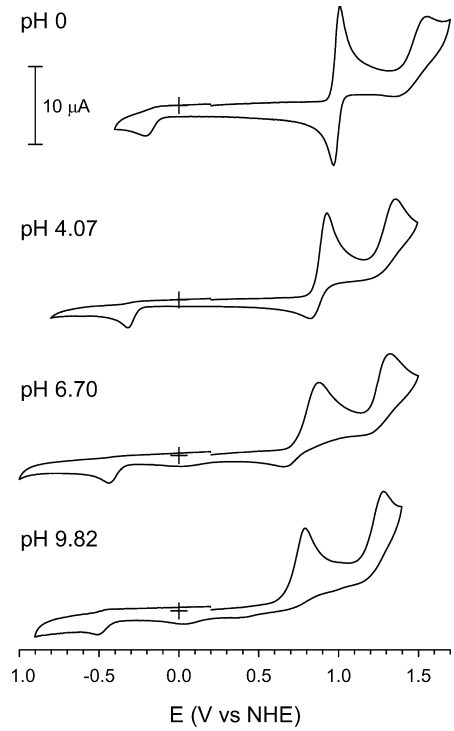

Figure 3. Cyclic voltammograms (25 mV s^{-1}) of 0.85 mM aqueous $Ru(bpy)_2(mpea)^{2+}$ solutions at various pH: 1.0 M H_2SO_4 (pH 0); acetate buffer (pH 4.07); phosphate buffer (pH 6.70); carbonate buffer (pH 9.82).

Spectroelectrochemistry was employed to obtain a more detailed picture of the transformations associated with wave **I**. For a set of UV−vis spectra acquired with a solution at pH ≥ 4 and electrolyzed at various potentials in wave **I**, principal component analysis indicated three absorbing species, consistent with an EE mechanism. The EE mechanism was employed to map the principal components and their scores to spectra and concentrations; the formal reduction potentials were optimized to provide the best agreement with the experimental spectra (Figure 4). Details of the spectroelectrochemical analysis are provided in the Supporting Information. The variations of the spectroelectrochemical formal potentials with pH yield parallel straight lines with slopes of −61 ± 1 mV, confirming that each step in the mechanism is a one-proton, one-electron process (see the Supporting Information). On the basis of these findings, the electrochemical transformations occurring in wave **I** at pH ≥ 4 correspond with sequential one-electron oxidations

(16) (a) Stratmann, R. E.; Scuseria, G. E.; Frisch, M. J. *J. Chem. Phys.* **1998**, *109*, 8218–8224. (b) Bauernschmitt, R.; Ahlrichs, R. *Chem. Phys. Lett.* **1996**, *256*, 454–464. (c) Casida, M. E.; Jamorski, C.; Casida, K. C.; Salahub, D. R. *J. Chem. Phys.* **1998**, *108*, 4439–4449.
(17) (a) Rusanova, J.; Rusanov, E.; Gorelsky, S. I.; Christendat, D.; Popescu, R.; Farah, A. A.; Beaulac, R.; Reber, C.; Lever, A. B. P. *Inorg. Chem.* **2006**, *45*, 6246–6262. (b) Fantacci, S.; De Angelis, F.; Selloni, A. *J. Am. Chem. Soc.* **2003**, *125*, 4381–4387. (c) Gorelsky, S. I.; Lever, A. B. P. *Can. J. Anal. Sci. Spectros.* **2003**, *48*, 93–105.
(18) (a) Barolo, C.; Nazeeruddin, M. K.; Fantacci, S.; Di Censo, D.; Comte, P.; Liska, P.; Viscardi, G.; Quagliotto, P.; De Angelis, F.; Ito, S.; Grätzel, M. *Inorg. Chem.* **2006**, *45*, 4642–4653. (b) Monat, J. E.; Rodriguez, J. H.; McCusker, J. K. *J. Phys. Chem. A* **2002**, *106*, 7399–7406.
(19) (a) Barone, V.; Cossi, M. *J. Phys. Chem. A* **1998**, *102*, 1995–2001. (b) Cossi, M.; Rega, N.; Scalmani, G.; Barone, V. *J. Comput. Chem.* **2003**, *24*, 669–681.
(20) Kelly, C. P.; Cramer, C. J.; Truhlar, D. G. *J. Phys. Chem. B* **2006**, *110*, 16066–16081.
(21) Tissandier, M. D.; Cowen, K. A.; Feng, W. Y.; Gundlach, E.; Cohen, M. J.; Earhart, A. D.; Coe, J. V. *J. Phys. Chem. A* **1998**, *102*, 7787–7794.

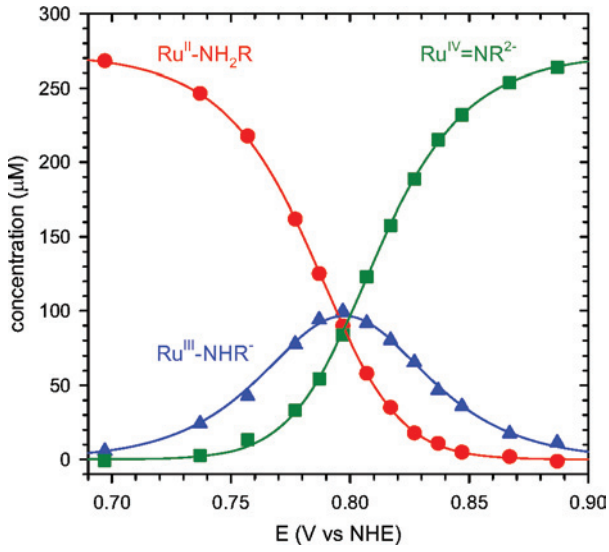

Figure 4. Spectroelectrochemical concentration profiles for electrolysis of 0.27 mM Ru(bpy)$_2$(mpea)$^{2+}$ in aqueous acetate buffer (pH 4.98). Curves represent predictions for an EE mechanism with $E^{\circ\prime}_1 = 0.800$ V and $E^{\circ\prime}_2 = 0.795$ V. The collection of experimental spectra at various potentials was analyzed by principal component analysis, and the loadings were mapped to concentrations, which are shown as points.

of the starting Ru(bpy)$_2$(mpea)$^{2+}$ complex (Ru^{II}−NH$_2$R) to an amidoruthenium(III) complex (Ru^{III}−NHR$^-$) and then an imidoruthenium(IV) (Ru^{IV}=NR^{2-}) complex.[22] The C(CH$_3$)$_2$-(py) portion of the mpea ligand is represented by R, and the charge in the upper right is the formal charge on the nitrogen.

It was not possible to obtain reproducible spectroelectrochemical data between pH 1 and 4, owing to slow disproportionation of the complex (see below), and consequently, we relied upon cyclic voltammetric data in this region. In the region from pH 1.0 to 2.2, the half-wave potential was found to vary linearly with pH with a slope of -27 ± 3 mV, as shown by the circles in Figure 5.[23] In this pH range, wave **I** corresponds with a two-electron oxidation with the loss of a single proton, consistent with oxidation of Ru^{II}−NH$_2$R to an amidoruthenium(IV) complex (Ru^{IV}=NHR$^-$). Spectroelectrochemical data in 1 M H$_2$SO$_4$ revealed only two absorbing species (isosbestic points at 269, 298, and 327 nm) and was accurately described by a simple two-electron process. In strongly acidic solution, no significant concentration of a Ru(III) species exists; the formal potential for the Ru(III)/Ru(II) couple is substantially more positive than that for the Ru(IV)/Ru(III) couple. This difference in formal potentials is sufficiently large that the maximum pK_a for Ru^{III}=NH$_2$R is approximately zero (see Supporting Information).

The lines for the pH-dependence of the cyclic voltammetry $E_{1/2}$ and spectroelectrochemical $E^{\circ\prime}$ data (Figure 5) intersect

(22) Although the kinetics for the proton-coupled electron transfer are slow in this pH region (pH 4−7), spectroelectrochemical measurements were performed over sufficiently long times (40−60 min between points) to permit equilibration. Above pH 7, however, the kinetics were too slow for equilibration even on this time scale, thus establishing an upper limit on the pH range for which reliable data could be obtained.

(23) The half-wave potentials were acquired at low sweep rates (9−100 mV s^{-1}) where the values were found to be independent of the sweep rate. Although wave **I** is quasireversible in this pH region (pH < 2.2), the half-wave potentials provide reasonable approximations of the values that would be obtained were the system reversible.

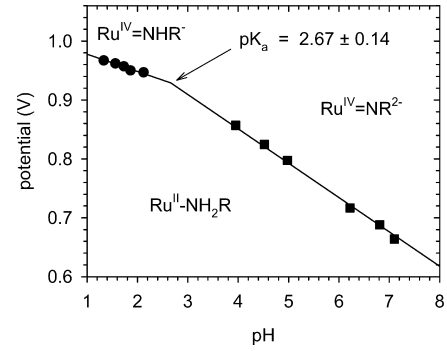

Figure 5. Variation of the reduction potential for wave **I** with pH. Circles represent half-wave potentials from cyclic voltammetry; squares represent formal potentials from spectroelectrochemical data. The slopes of the lines represent ideal responses expected for 2e$^-$/1H$^+$ (pH < 2.67) and 2e$^-$/2H$^+$ (pH > 2.67) processes.

at pH 2.67 ± 0.14, which corresponds with the pK_a of the Ru^{IV}=NHR$^-$ species. To verify this conclusion, we prepared a solution of Ru^{IV}=NR^{2-} at pH 7 (phosphate buffer) by exhaustive electrolysis of [Ru(bpy)$_2$(mpea)]$^{2+}$. At this pH, the imidoruthenium(IV) complex is stable in solution for many hours. Aliquots of this solution were mixed with a low pH phosphate buffer to obtain final solutions in the pH range from 1.2 to 4.3. The UV−vis spectra of the final solutions were recorded immediately after preparation before significant disproportionation could occur. The analysis of the resulting set of spectra at varying pH, which principal component analysis showed to contain only two absorbing species (isosbestic points at 295, 330, and 451 nm), yielded a pK_a of 2.62 ± 0.06 in good agreement with the electrochemical data. The spectrum of the protonated complex matches the spectrum of Ru^{IV}=NHR$^-$, obtained by spectroelectrochemistry in 1 M H$_2$SO$_4$. The reactivity of this system is summarized by the reactions listed in Table 1 (experimental data).

The Ru^{IV}=NHR$^-$ complex is stable in 1 M H$_2$SO$_4$ for several hours, and the Ru^{IV}=NR^{2-} complex is stable for longer periods in solutions between pH 4 and 9. Mixtures of Ru^{IV}=NHR$^-$ and Ru^{IV}=NR^{2-}, however, are much less stable. In the pH range 1 to 4, solutions of the Ru(IV) complex contain significant amounts of [Ru(bpy)$_2$(mpea)]$^{2+}$ and [Ru(bpy)$_2$(mpeNO)]$^{2+}$ (Ru^{II}−NOR) after 20 min. Our attempts to isolate the Ru(IV) complexes as hexafluorophosphate salts were unsuccessful; the isolated solids always consisted of mixtures of [Ru(bpy)$_2$(mpea)](PF$_6$)$_2$ and [Ru(bpy)$_2$(mpeNO)](PF$_6$)$_2$.

Computational Analysis. Density functional computations, b3lyp/cpcm/cep-31g(d), were performed to aid in elucidating the electronic structures and reactivities of the various species in this system. The spectroscopic data for related systems indicates the existence of significant specific solvation effects at the NH$_2$ site, and for this reason, our models included one water molecule at each hydrogen bonding site.[1,24] We did not perform an exhaustive survey of the distribution of orientations of the water molecules; in most cases, the energy is based upon a single optimized geometry. Computed free energies in aqueous solution were used to calculate the standard reduction potentials

(24) Curtis, J. C.; Sullivan, B. P.; Meyer, T. J. *Inorg. Chem.* **1983**, *22*, 224–236.

Table 1. Calculated and Experimental Thermodynamic Properties

	property	
	calcd[a]	exptl
reaction	$E°$ (V vs NHE)	$E°$ (V vs NHE)[b]
$Ru^{III}—NH_2R + e^- \rightleftarrows Ru^{II}—NH_2R$	1.32	
$Ru^{III}—NHR^- + H^+ + e^- \rightleftarrows Ru^{II}—NH_2R$	0.78	1.082 (±0.003)
$Ru^{IV}=NHR^- + H^+ + 2e^- \rightleftarrows Ru^{II}—NH_2R$	1.18	1.007 (±0.002)[c]
$Ru^{IV}=NHR^- + e^- \rightleftarrows Ru^{III}—NHR^-$	1.57	0.932 (±0.005)
$Ru^{IV}=NR^{2-} + 2H^+ + 2e^- \rightleftarrows Ru^{II}—NH_2R$	1.15	1.085 (±0.004)
$Ru^{IV}=NR^{2-} + H^+ + e^- \rightleftarrows Ru^{III}—NHR^-$	1.52	1.087 (±0.005)
$Ru^{V}=NR^{2-} + e^- \rightleftarrows Ru^{IV}=NR^{2-}$	1.41	
$Ru^{VI}=NR^{2-} + e^- \rightleftarrows Ru^{V}=NR^{2-}$	3.29	
$Ru^{II}—NOR + 4H^+ + 4e^- \rightleftarrows Ru^{II}—NH_2R + H_2O(l)$	0.65	
$Ru^{II}—NOR + e^- \rightleftarrows Ru^{II}—NOR^-$	−0.32	
$Ru^{II}—NOR + H^+ + e^- \rightleftarrows Ru^{II}—NOHR$	0.12	
$Ru^{II}—NOR + H^+ + e^- \rightleftarrows Ru^{II}—NHOR$	−0.79	
$Ru^{II}—NOHR + e^- \rightleftarrows Ru^{II}—NOHR^-$	−0.81	
$Ru^{II}—NOHR + H^+ + e^- \rightleftarrows Ru^{II}—NHOHR$	0.17	
$Ru^{II}—NHOHR + e^- \rightleftarrows Ru^{II}—NHOHR^-$	−1.37	
$Ru^{II}—NHOHR + H^+ + e^- \rightleftarrows Ru^{III}—NHR^- + H_2O(l)$	1.55	
	pK_a	
$Ru^{III}—NH_2R \rightleftarrows Ru^{III}—NHR^- + H^+$	−9.1	≤0
$Ru^{IV}=NHR^- \rightleftarrows Ru^{IV}=NR^{2-} + H^+$	−0.9	2.62 (±0.06)

[a] Calculated by b3lyp/cpcm/cep-31g(d) with explicit water molecules added. [b] Formal potential for 1 M H^+. [c] Value obtained from half-wave potentials.

and the equilibrium constants (see Supporting Information). The standard reduction potentials are reported versus NHE using our calculated value of $E_{NHE} = 4.28$ V, which may be compared with the accepted value of 4.44 V.[25,26] The limited basis set (a double-ζ basis set with a single set of diffuse functions on the second row nonmetals), the solvation model, and the limited number of water configurations all contribute to the error in G°. Where experimental values are available for comparison, the average absolute error in ΔG° is 34 kJ with the greatest error being 63 kJ. Relative to the computed G° values for $Ru^{II}—NH_2R$ and $Ru^{IV}=NR^{2-}$, the G° for $Ru^{III}—NHR^-$ is substantially lower (37 kJ) than expected, while the value for $Ru^{IV}=NHR^-$ is some 23 kJ too high. Errors of this magnitude are not unexpected for systems involving transition metals, relatively limited basis sets, and solvation models,[27] and it is not unreasonable that errors for open-shell systems may differ significantly from those for closed-shell systems. For the purposes of this study, however, these thermodynamic quantities are sufficiently accurate to permit valuable inferences regarding the mechanism for redox transformations involving the amine site. The calculated standard reduction potentials and the acid dissociation constants for various relevant reactions are listed in Table 1.

The molecular orbital description for the $Ru^{II}—NH_2R$ complex shows fully occupied d_{xy} (homo), d_{yz}, and d_{xz} orbitals that are primarily nonbonding and lie just above the pyridyl π_3 orbitals.[28] The lowest unoccupied orbitals are pyridyl π_4* and π_5* orbitals, with the Ru−N σ* orbitals (d_{z^2} and d_{x^2}) mixed with the π_5* orbitals. Oxidation and deprotonation yields the $Ru^{III}—NHR^-$ complex, which possesses a partial metal−nitrogen π bond. Formally, the complex is an amidoruthenium(III) species, but the Mulliken analysis (see the Supporting Information) is the intermediate between a d^5 and d^6 ruthenium, and the spin density is approximately equally distributed across the Ru−N linkage.[29]

Further oxidation produces $Ru^{IV}=NHR^-$, in which the LUMO is the Ru=N π* orbital (d_{yz}) and there is a full π bond between the metal and the amide nitrogen. The only occupied metal-centered orbitals are the d_{xz} and the d_{xy}, each showing weak π bonding interactions with the pyridyl ligands, corresponding with a d^4 Ru(IV) complex. Deprotonation of $Ru^{IV}=NHR^-$ releases a second pair of electrons on the nitrogen for π interaction with the metal. In this case, however, both π and π* (d_{xz}) orbitals are fully occupied, and there is a net single Ru=N π bond involving the d_{yz} orbital. The explicit water of solvation is oriented to donate a hydrogen bond to the $Ru^{IV}=NR^{2-}$ imido site.

The $Ru^{II}—NOR$ complex shows a d^6 configuration, with occupied nonbonding d_{xy} and d_{xz} orbitals. There is π delocalization across the Ru=N=O linkage, with the Ru=N π interaction arising from back-bonding from the Ru d_{yz} orbital and from the LUMO being the N=O π* orbital.

Spectroscopy. The electronic spectra for $[Ru(bpy)_2(mpea)]^{2+}$ (Figure 6) display three bands. The bands at 342 and 475 nm are metal-to-ligand charge transfer (MLCT) transitions while the UV band at 289 nm consists of both MLCT and pyridyl $\pi \rightarrow \pi$* transitions. The energies of the MLCT transitions for $[Ru(bpy)_2(mpea)]^{2+}$ show a significant solvent dependence, which provides evidence for the existence of important hydrogen bonding interactions between the solvent and the $Ru—NH_2$ site. Kamlet−Taft parameters for the MLCT transitions for $[Ru(bpy)_2(mpea)]^{2+}$ are compared with those for *meso*-$[Ru(dipa)_2]^{2+}$ (dipa = di(2-pyridyl)methanamine) in Table 2.[30] The two complexes have the same charge and are of similar size and structure; consequently, the solvent polarity effects (p) are similar. However, effects associated with the ability of the solvent to accept a hydrogen bond (b) are only half as strong for $[Ru(bpy)_2(mpea)]^{2+}$, which possesses a single NH_2 site, compared with *meso*-$[Ru(dipa)_2]^{2+}$, which possesses two NH_2 sites.[31]

Spectra calculated for the various complexes are compared with the experimental spectra in Figure 6, and the dominant character of the various transitions are listed in Table 3. As

(25) Trasatti, S. *Pure Appl. Chem.* **1986**, *58*, 955–966.
(26) Richardson, D. E. In *Comprehensive Coordination Chemistry II*; McCleverty, J. A., Meyer, T. J., Eds.; Elsevier: New York, 2004; Vol. 2, pp 633−642.
(27) Baik, M.-H.; Friesner, R. A. *J. Phys. Chem. A* **2002**, *106*, 7407–7412.
(28) The coordinate system is chosen so that the $Ru—NH_2$ bond lies along the z axis and the Ru−N bond for the mpea pyridyl group lies along the x axis.
(29) The nitrogen is the more electronegative element in the Ru−N bond and therefore is regarded as having sole ownership of the shared electrons for the purpose of assigning formal charges and oxidation states.
(30) Kamlet, M. J.; Abboud, J.-L.; Abraham, M. H.; Taft, R. W. *J. Org. Chem.* **1983**, *48*, 2877–2887.
(31) There are weak effects associated with the ability of the solvent to donate a hydrogen bond (a). These effects, which likely arise from solvent interactions with the pyridyl ligands, are similar in magnitude for the two complexes.

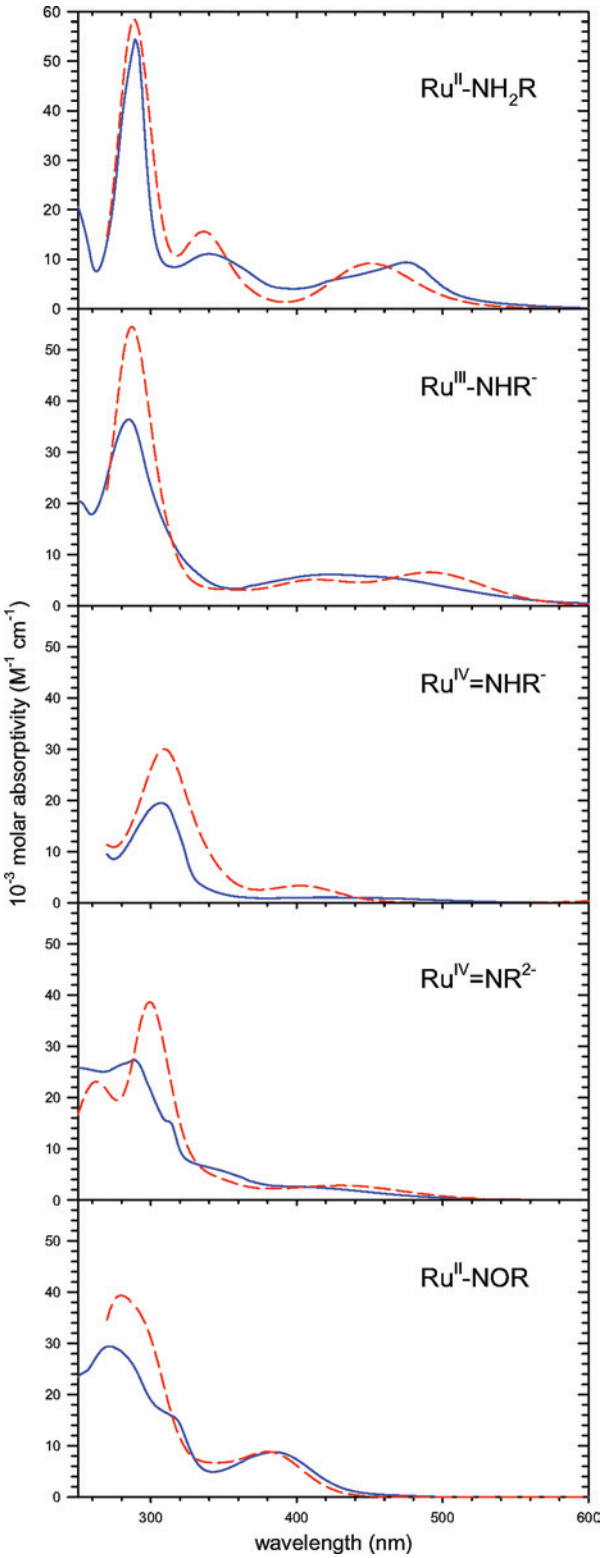

Figure 6. Experimental (solid blue) and b3lyp/cep-31g(d) (dashed red) electronic spectra of complexes in water.

is expected for a system of this size and complexity, there is considerable mixing of transitions, especially in the UV region, that prevents simple assignment of transitions. In general, though, the UV transitions (280−309 nm) are the most intense bands and involve substantial pyridyl $\pi \rightarrow \pi^*$ character. All of the transitions, both UV and visible, involve significant metal-based orbitals in the ground state, the excited state, or both. For the amido Ru(III) and Ru(IV) complexes, excitations to the Ru−N σ^* orbital (involving pyridyl nitrogens) are observed. As described above, the Ru^{III}−NHR$^-$, the Ru^{IV}=NHR$^-$, and the Ru^{IV}=NR^{2-} complexes all involve a partial or full Ru=N π bond, and the π and π^* orbitals for this bond figure prominently in the electronic spectra of these complexes. Interestingly, the UV band for Ru^{III}−NHR$^-$ includes contributions from occupied pyridyl π orbitals *to* the partially occupied Ru=N π^* orbital and transitions *from* the Ru=N π^* orbital to the pyridyl π^* orbitals. The Ru(IV) complexes involve one or the other of these transitions but not both. The Ru^{III}−NHR$^-$ complex also undergoes a Ru=N $\pi \rightarrow \pi^*$ transition in the visible region, which is effectively an MLCT transition since the Ru=N π orbital is predominantly Ru d_{yz} and the Ru=N π^* orbital (the LUMO for β electrons) predominantly nitrogen p_y in character.

Mechanism for the Formation of Ru^{II}−NOR. The formation of the nitrosoruthenium(II) complex requires the nucleophilic attack of water at the amido or imido nitrogen, and this attack does not readily occur for the Ru^{IV}=NHR$^-$ and Ru^{IV}=NR^{2-} complexes, as evidenced by their stability in aqueous solution and by the presence of an additional anodic wave (**II**) in the cyclic voltammetry. The key step in nitroso formation must be the oxidation of the Ru(IV) complex to either a Ru(V) or Ru(VI) complex, which is susceptible to attack by water. The b3lyp/cpcm/cep-31g(d) computations give $E^\circ = 1.41$ and 3.29 V for the Ru^{V}=NR^{2-}/Ru^{IV}=NR^{2-} and the Ru^{VI}=NR^{2-}/Ru^{V}=NR^{2-} couples, respectively, indicating that the Ru(VI) state is too high in energy to be reached, and thus, Ru^{V}=NR^{2-} is the reactive intermediate. It should be noted that the anodic peak potential for wave **II** occurs near 1.5 V in 1 M H_2SO_4, which is consistent, within the computational accuracy, with the E° predicted for the Ru^{V}=NR^{2-}/Ru^{IV}=NHR$^-$ couple.

As reported above, the Ru^{IV}=NHR$^-$ and the Ru^{IV}=NR^{2-} species are individually stable for hours in aqueous solution while Ru^{II}−NOR and Ru^{II}−NH$_2$R can be found in solutions containing mixtures of these species in less than half an hour. Disproportionation of either Ru(IV) species is thermodynamically unfavorable, but the highly reactive Ru^{V}=NR^{2-} intermediate is rapidly converted to the nitroso product, shifting the position of the disproportionation equilibrium. The controlling factor may be the relatively slow kinetics for the proton-coupled electron transfer in this system (Figure 3). Disproportionation of either Ru^{IV}=NHR$^-$ or Ru^{IV}=NR^{2-} requires a proton transfer and is thus very slow, but the cross reaction

$$\mathrm{Ru^{IV}{=}NHR^- + Ru^{IV}{=}NR^{2-} \rightleftarrows Ru^{III}{-}NHR^- + Ru^{V}{=}NR^{2-}} \quad (1)$$

requires no proton transfer and should therefore occur more rapidly. In the range from pH 1 to 4, where solutions contain significant mixtures of Ru^{IV}=NHR$^-$ and Ru^{IV}=NR^{2-}, eq 1 provides a route for creating the highly reactive Ru^{V}=NR^{2-} intermediate necessary for formation of [Ru^{II}(bpy)$_2$(mpeNO)]$^{2+}$.

Table 2. Kamlet−Taft Parameters

	$Ru(bpy)_2(mpea)^{2+}$		*meso*-$Ru(dipa)_2^{2+}$[a]	
ν_0 (10^3 cm^{-1})	21.57 ± 0.04	29.76 ± 0.08	24.18 ± 0.06	27.44 ± 0.06
p (cm^{-1})	−480 ± 50	−560 ± 90	−650 ± 60	−590 ± 60
b (cm^{-1})	−570 ± 30	−510 ± 50	−1090 ± 60	−1020 ± 60
a (cm^{-1})	87 ± 18	120 ± 40	87 ± 26	163 ± 26

[a] dipa = di(2-pyridyl)methanamine. Parameters from ref 1.

Table 3. Electronic Transitions in Water

	experimental λ_{max}/nm (ε/M^{-1} cm^{-1})	calcd[a] λ_{max}/nm	dominant character			
Ru^{II}−NH_2R	289 (54400)	289	py $\pi \rightarrow \pi^*$	Ru d → py π^*		
	342 (11100)	336		Ru d → py π^*		
	475 (9380)	451		Ru d → py π^*		
Ru^{III}−NHR^-	286 (36300)	287	py $\pi \rightarrow \pi^*$	Ru d → py π^*	py $\pi \rightarrow$ Ru=N π^*	Ru=N $\pi^* \rightarrow$ py π^*
	427 (5700)	414		Ru d → py π^*		Ru d → Ru−N_{py} σ^*
		490				Ru=N $\pi \rightarrow$ Ru=N π^*
Ru^{IV}=NHR^-	307 (27800)	309	py $\pi \rightarrow \pi^*$		py $\pi \rightarrow$ Ru=N π^*	py $\pi \rightarrow$ Ru−N_{py} σ^*
	418 (1600)	402			py $\pi \rightarrow$ Ru=N π^*	
Ru^{IV}=NR^{2-}	289 (25600)	299	py $\pi \rightarrow \pi^*$	Ru d → py π^*		
		429				Ru=N $\pi^* \rightarrow$ py π^*
Ru^{II}−NOR	271 (29400)	280	py $\pi \rightarrow \pi^*$	Ru d → py π^*		Ru=N π/N=O $\pi^* \rightarrow$ py π^*
	384 (8770)	380		Ru d → py π^*		

[a] Calculated by b3lyp/cep-31g(d) with explicit water molecules added. The calculated transition energies are shifted by −0.13 eV to make the calculated λ_{max} for the most intense $Ru(bpy)_2(mpea)^{2+}$ band coincide with the experimental value of 289 nm.

Table 4. NBO Atomic Charges[a]

	NBO atomic charge	
	Ru	N
Ru^{II}−NH_2R	0.60	−0.83
Ru^{III}−NHR^-	0.70	−0.58
Ru^{IV}=NHR^-	0.89	−0.39
Ru^{IV}=NR^{2-}	0.79	−0.35
Ru^{V}=NR^{2-}	0.95	−0.08
Ru^{VI}=NR^{2-}	1.04	0.07
Ru^{II}−NOR	0.68	0.13
Ru^{II}−NOHR	0.61	−0.07
Ru^{II}−NHOHR	0.59	−0.31

[a] Calculated by b3lyp/cpcm/cep-31g(d) with explicit water molecules added. Atomic charges obtained from natural bond order (NBO) analysis.[37]

The progressive oxidation of the original Ru^{II}−NH_2R complex increases the atomic charge of the amine nitrogen (Table 4). In the Ru^{IV}=NR^{2-} complex, the nitrogen is still sufficiently negative in charge that it is stabilized by donation of a hydrogen bond from water. In contrast, water placed near the imido nitrogen (in either orientation) is ejected from that site in geometry optimizations for Ru^{V}=NR^{2-} and Ru^{VI}=NR^{2-}; interactions between water and the methyl and the pyridyl hydrogens are stronger than interactions with the imido site. In order to explore the susceptibility of the imidoruthenium(V) species to nucleophilic attack by water, a water molecule was placed at a fixed distance from the imido nitrogen, and the geometry of the system was optimized. Two other water molecules were placed off the attacking water, as illustrated at the top of Figure 7. With no constraint on the N···O distance, the three water molecules took up positions off the methyl groups well removed from the imido site. As the oxygen of the water was brought closer to the imido nitrogen, a transition state was found at a N···O distance of 1.936 Å, leading to a stable intermediate with an optimized N−O bond length of 1.496 Å (no constraints on the geometry optimization). For comparison, a N=O bond length of 1.240 Å was calculated for the Ru^{II}−NOR complex. When solvation effects and thermal contributions were taken into account, $\Delta G^{\ddagger} = 12$ kJ mol^{-1} for this reaction, consistent with a highly reactive imidoruthenium(V) intermediate.[32]

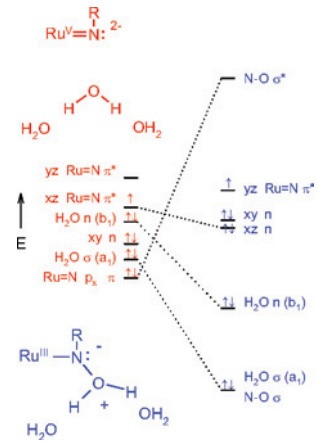

Figure 7. Simplified b3lyp/cep-31g(d) molecular orbital diagram for attack of Ru^{V}=NR^{2-} by water. The orbitals for the two water molecules solvating the attacking water are not shown. The Lewis structures at the top and bottom represent the reactants (red, left) and products (blue, right), respectively.

We did not perform an extensive search for other transition states; thus, a lower energy route may exist. Even given the errors inherent in the computed energies, it seems clear that the Ru^{V}=NR^{2-} species reacts very quickly with water. The "hydrated" complex, Ru^{III}−NR−OH_2, is predicted to be a

(32) We performed a similar computation using the Ru^{IV}=NR^{2-} complex but were unable to find a transition state or a stable intermediate. Reducing the N···O distance from 2.93 Å (the distance for the water solvating the imido group) to 1.80 Å increased the standard free energy by over 100 kJ mol^{-1}.

(33) The oxygen is much more basic than the nitrogen in Ru^{II}−NOR^-, and protonation thus occurs at the oxygen.

(34) Moyer, B. A.; Meyer, T. J. *Inorg. Chem.* **1981**, *20*, 436–444.
(35) Murphy, W. R., Jr.; Takeuchi, K.; Barley, M. H.; Meyer, T. J. *Inorg. Chem.* **1986**, *25*, 1041–1053.
(36) (a) Chui, W.-H.; Cheung, K.-K.; Che, C.-M. *J. Chem. Soc., Chem. Commun.* **1995**, 441–442. (b) Chiu, W.-H.; Peng, S.-M.; Che, C.-M. *Inorg. Chem.* **1996**, *35*, 3369–3374.
(37) Glendening, E. D.; Reed, A. E.; Carpenter, J. E.; Weinhold, F. *NBO*, version 3.1. Implemented with Gaussian03.

strong acid; therefore, the actual reaction pathway, which would presumably have a lower $\Delta G^{\ddagger}$, would involve attack by water with the concomitant loss of a proton to yield $Ru^{II}-NR-OH$ (a ruthenium(II)-bound hydroxylamine radical), which is readily oxidized and deprotonated to produce the ultimate nitrosoruthenium(II) product.

$$Ru^{V}{=}NR^{2-} + H_2O \rightarrow Ru^{II}-NR-OH + H^+ \qquad (2)$$

$$Ru^{II}-NR-OH \rightleftarrows Ru^{II}-NOR + H^+ + e^- \qquad (3)$$

The character of the attack by H_2O on $Ru^{V}{=}NR^{2-}$ is illustrated in the molecular orbital diagram in Figure 7. The initial Ru=N bond order is 2.5, arising from a full π bond involving the Ru d_{yz} orbital and a partial π bond involving the Ru d_{xz} orbital. The HOMO is this partially occupied Ru=N π^* orbital, which is predominantly Ru d_{xz} in character; the corresponding Ru=N π orbital is predominantly N p_x in character. One lobe of the singly occupied d_{xz} Ru=N π^* is exposed for interaction with the water b_1 (n) and a_1 (H−O σ) orbitals, and the ultimate N=O bond will occupy this position. In our simulations, however, the approaching water did not lie perfectly in the *yz* plane but instead approached from the side, interacting with both the d_{xz} and the d_{yz} Ru=N π^* orbitals. This interaction feeds electron density into the Ru=N π^* orbitals, lengthening the Ru−N bond (from 1.776 to 1.965 Å) and weakening the Ru=N π bonding. The Ru d_{xz} orbital drops in energy, becoming nonbonding and fully occupied, while the nitrogen p_x (formerly Ru=N π) and the water a_1 orbitals mix to give N−O σ and σ^*. The net result is donation of electron density from the oxygen to the nitrogen to create a N−O σ bond and formal reduction of the metal by the nitrogen to yield a d^5 Ru^{III} complex with a partial Ru=N π bond (bottom of Figure 7). Although depicted in the figure as the simple addition of water to the complex, the actual process likely involves the concerted loss of a proton. Deprotonation of the water allows the oxygen to participate in the π system and releases additional electron density to the nitrogen and ruthenium. Although the spin density is distributed along the partially occupied Ru=N=O π^* orbital, its highest concentration is upon the nitrogen, and the species is best regarded as a Ru^{II}-bound hydroxylamine radical.

Mechanism for the Reduction of $Ru^{II}-NOR$. The electrochemically irreversible reduction of $[Ru(bpy)_2(mpeNO)]^{2+}$ to $[Ru(bpy)_2(mpea)]^{2+}$ occurs at relatively negative potentials ($E_{pc} = -0.19$ V in 1 M H_2SO_4 at 9 mV s^{-1}). At sweep rates up to 1 V s^{-1}, we were unable to identify intermediates or observe an anodic peak on the reverse scan of wave **III**. The initial reduction product and any subsequent intermediates must react quickly to form the $Ru^{II}-NH_2R$ complex. The $Ru^{II}-NOR$ LUMO is the N=O π^* orbital (with weak Ru=N π^* character), and reduction of the complex begins by populating this orbital and protonating the oxygen to yield the $Ru^{II}-NOHR$ complex described above.[33] The calculated E° for this process, which is simply the reverse of the oxidation process in eq 3, is 0.12 V. The $Ru^{II}-NOHR$ HOMO is the partially occupied Ru=N π^*/N=O π^* orbital, which is predominantly nitrogen in character; reduction and protonation destroys the Ru=N=O π interactions, leading to a hydroxylamineruthenium(II) complex ($Ru^{II}-NHOHR$) (calcd $E^\circ = 0.17$ V).

For the first two reductions, the site of reduction and the site of protonation are the same, (the NO site) and consequently, the reduction is proton-coupled. For the $Ru^{II}-NHOHR$ complex, however, the LUMO is a bipyridine π^* orbital while the most basic site is the OH site; thus, reduction and protonation are not directly coupled. Reduction of a Ru(II)-bound bipyridine ligand is energetically unfavorable ($E^\circ = -1.37$ V calculated for this case); thus, the next step in the reduction process is protonation of the hydroxylamine. No stable $Ru^{II}-NHOH_2R^+$ complex could be found, however. Geometry optimization leads to the ejection of water to produce the amidoruthenium(IV) complex, which is readily reduced to $Ru^{II}-NH_2R$ at potentials where $Ru^{II}-NHOHR$ is generated. This behavior is consistent with $Ru^{IV}{=}NHR^-$ being unreactive toward attack by water, as described above.

$$Ru^{II}-NHOHR + H^+ \rightleftarrows Ru^{IV}{=}NHR^- + H_2O \qquad (4)$$

Discussion

The formal potentials and acid−base chemistry for the oxidative transformations of $[Ru^{II}(bpy)_2(mpea)]^{2+}$ in wave **I** are similar to those for $[Ru^{II}(bpy)_2(py)(OH_2)]^{2+}$ (py = pyridine), especially at higher pH: 0.675 V for $Ru^{IV}{=}NR^{2-}$/$Ru^{III}-NHR^-$ and 0.670 V for $Ru^{III}-NHR^-/Ru^{II}-NH_2$ compared with 0.73 V for $Ru^{IV}{=}O^{2-}/Ru^{III}-OH^-$ and 0.66 V for $Ru^{III}-OH^-/Ru^{II}-OH_2$ at pH 7.[34] A notable difference in behavior is the acidity of $Ru^{IV}{=}OH^-$, which is not observed even in 1 M H^+, while the pK_a for $Ru^{IV}{=}NHR^-$ is 2.62. By contrast, $Ru^{III}-NH_2R$ is more acidic (p$K_a \leq 0$) than $Ru^{III}-OH_2$ (p$K_a = 0.85$). In addition to the inherent differences in basicity between NH_2R and OH_2, these differences likely reflect differences in the strengths of the π-bonding interactions, which stabilize the deprotonated form of the complex. The better energy match between the Ru d and N p orbitals facilitates a stronger π interaction in $Ru^{III}-NHR^-$ than in $Ru^{III}-OH^-$, resulting in greater acidity for $Ru^{III}-NH_2R$ compared with $Ru^{III}-OH_2$. While the d_{yz}-p_y π bonding is stronger for Ru=N compared with that of Ru=O, the d_{xz}-p_x π bonding is much weaker owing to hindrance from the remainder of the mpea ligand. This hindrance is not present in the $Ru^{IV}{=}O^{2-}$ complex.

The reaction pathways between $[Ru^{II}(bpy)_2(mpea)]^{2+}$ and $[Ru^{II}(bpy)_2(mpeNO)]^{2+}$ are illustrated in Scheme 1. Of the eight species in this mechanism, five have been identified experimentally ($Ru^{II}-NH_2$, $Ru^{III}-NHR^-$, $Ru^{IV}{=}NHR^-$, $Ru^{IV}{=}NR^{2-}$, and $Ru^{II}-NOR$), and their spectra are depicted by the blue curves in Figure 6. The remaining three species ($Ru^{V}{=}NR^{2-}$, $Ru^{II}-NOHR$, and $Ru^{II}-NHOHR$), all of which are expected to be short-lived, are proposed on the basis of density functional computations. This mechanism is similar to those proposed for oxidative transformations of ammonia in $[Ru(bpy)(tpy)NH_3]^{2+}$ and $[Os(bpy)(tpy)NH_3]^{2+}$.[35] Interestingly, the complex subject to attack by water differs: an imidoruthenium(IV) species, $[(tpy)(bpy)Ru^{IV}{=}NH]^{2+}$, and a

Scheme 1

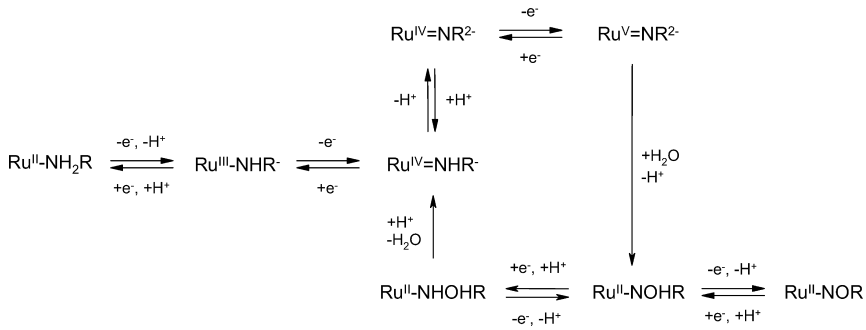

nitridoosium(V) species, $[(tpy)(bpy)Os^{V}{\equiv}N]^{2+}$, in contrast with the imidoruthenium(V) species found in the mpea system. The transformation of a ruthenium-bound amine to a nitrosoalkane has also been reported for the 2,3-diamino-2,3-dimethylbutane ligand.[36] In that case, an imidoruthenium(V) intermediate was observed via cyclic voltammetry, whereas chemical oxidation with Ce^{4+} yielded the dinitroso complex, a process reported to occur through an imidoruthenium(VI) intermediate.

The precise nature of the species subject to nucleophilic attack by water is of interest, and a diverse range of behaviors have been reported. The susceptibility of a complex to such attack is controlled by the partial charge on the nitrogen and the existence of favorable frontier orbital interactions. Progressive oxidation of the metal draws electron density away from the nitrogen, ultimately producing an approximately neutral or slightly positive partial charge on the nitrogen that is conducive to attack by water. If the electron density around the nitrogen is too great, the energy barrier for an approaching water molecule is too high. This is the case for $Ru^{IV}{=}NR^{2-}$, while for $Ru^{V}{=}NR^{2-}$, the energy barrier is quite low, as described above.

The interaction of the water with the nitrogen requires the donation of electrons from the H_2O HOMO and/or HOMO-1 (b_1 and a_1, respectively) to an empty or singly occupied acceptor orbital, which is a Ru=N π^* orbital, of either d_{xz}-p_x or d_{yz}-p_y symmetry. The Ru=N d_{yz}-p_y interaction is stronger and that π^* orbital lies at a higher energy than the d_{xz}-p_x π^*, with these two orbitals being LUMO and LUMO$+1$ in $Ru^{V}{=}NR^{2-}$. In principle, either of the Ru=N π^* orbitals would be a suitable acceptor. For the mpea system, the methyl groups and one of the bpy ligands partially obstruct access to the d_{yz} Ru=N π^* orbital, but this steric interference is relatively modest and seems unlikely to be the dominating factor. The mere availability of the d_{yz} Ru=N π^* orbital is insufficient for attack by water, as evidenced by the stability of $Ru^{IV}{=}NHR^{-}$ and $Ru^{IV}{=}NR^{2-}$, each of which possess the empty d_{yz} Ru=N π^* orbital as the LUMO. In the oxidation sequence, the $Ru^{V}{=}NR^{2-}$ complex is the first to possess a partially filled d_{xz} Ru=N π^*, and the availability of this π^* as an acceptor orbital may be a significant factor.

The energy match between the H_2O b_1 and a_1 and the Ru=N π^* orbitals may be a more important factor. For the $Ru^{III}{-}NHR^{-}$, $Ru^{IV}{=}NHR^{-}$, and $Ru^{IV}{=}NR^{2-}$ complexes, the lowest lying empty or partially filled Ru=N π^* orbital is 5.7, 4.0, and 4.6 eV above the H_2O b_1 orbital, respectively. The H_2O b_1 energy is that for a water solvating the amide/imide site. In this system, these energy gaps may be too large for effective donor−acceptor interaction, especially given the electrostatic issues described above. In contrast, the energy gap is only 1.6 eV for the $Ru^{V}{=}NR^{2-}$ complex. The Ru d orbitals typically lie well above the H_2O b_1, but progressive oxidation of the metal lowers the Ru d energies, and for $Ru^{V}{=}NR^{2-}$, the H_2O b_1 orbital lies in the middle of the Ru d orbitals (Figure 7).

The mpea ligand was chosen for study because it is structurally similar to 2-aminomethylpyridine (ampy) and 2-(1-aminoethyl)pyridine (Meampy). An investigation of the kinetics of the oxidative dehydrogenation of $Ru(bpy)_2(ampy)^{2+}$and $Ru(bpy)_2(Meampy)^{2+}$ to the corresponding imine complexes has been reported.[8b] The kinetic model consists of a one-electron oxidation of the amineruthenium(II) complex to the amineruthenium(III) intermediate, which undergoes acid dissociation to yield an amidoruthenium(III) intermediate. Reaction between the amine- and amidoruthenium(III) intermediates yields the reactive amidoruthenium(IV) species, which quickly reacts to produce the imine product. The application of this kinetic model to experimental data yields a pK_a for the amineruthenium(III) species of 2.41 for the ampy complex and 2.39 and 1.89 for the $\Lambda S(\Delta R)$ and $\Lambda R(\Delta S)$ diastereoisomers of the Meampy complexes, respectively. These pK_a values are substantially higher than the p$K_a \leq 0$ obtained for $Ru(bpy)_2(mpea)^{3+}$ in this study (see the Supporting Information). Given the similar structures, one would expect the acidity of $Ru(bpy)_2(mpea)^{3+}$ to be similar to, or perhaps slightly higher, than that of $Ru(bpy)_2(ampy)^{3+}$ or $Ru(bpy)_2(Meampy)^{3+}$. Clearly, this is an issue that warrants further investigation. It is noteworthy that the estimates of the pK_a were obtained in very different ways: one from a kinetic model fit to flash photolysis data and the other from a thermodynamic model fit to electrochemical data.

The structures and reactivities of the $Ru^{IV}{=}NHR^{-}$ and $Ru^{IV}{=}NH^{2-}$ intermediates are also of interest. Crystal structures for amidoruthenium(IV) complexes of 2,3-diamino-2,3-dimethylbutane (L) have been reported.[36] Our attempts to isolate pure salts of $Ru^{IV}{=}NHR^{-}$ and $Ru^{IV}{=}NR^{2-}$ have yielded mixtures of $Ru^{II}{-}NH_2R$ and $Ru^{II}{-}NOR$. The $Ru^{IV}{=}NHR^{-}$ and $Ru^{IV}{=}NR^{2-}$ species are not thermodynamically stable; their persistence for hours in aqueous solution is attributable to the absence of a facile pathway

for reaction. In solutions near pH 2.6 and during the precipitation process, kinetically favorable pathways for disproportionation are available. Instability toward disproportionation was not reported for $Ru^{IV}(L)(L-H)_2^{2+}$ and $Ru^{IV}(bpy)(L-H)_2^{2+}$. At pH 4, the Ru(IV/II) reduction potentials for $Ru^{IV}(L)(L-H)_2^{2+}$ and $Ru^{IV}(bpy)(L-H)_2^{2+}$ are 0.25 and 0.54 V, respectively, whereas the corresponding potential for $Ru^{IV}{=}NR^{2-}$ is 0.85 V. The progressive replacement of aliphatic amine ligands (good σ-donors, no π-acceptor character) with pyridyl ligands (poor σ-donors, good π-acceptors) removes electron density from the Ru(II), leading to increasingly high reduction potentials. The substantially higher reduction potential for $Ru^{IV}{=}NR^{2-}$ reflects a more electron-deficient Ru−N site, providing greater oxidizing potential and a nitrogen more susceptible to nucleophilic attack by water.

Conclusions

As illustrated in Scheme 1, the redox pathways between $[Ru^{II}(bpy)_2(mpea)]^{2+}$ and $[Ru^{II}(bpy)_2(mpeNO)]^{2+}$ have been identified, and three important reactive intermediates ($Ru^{III}-NHR^-$, $Ru^{IV}{=}NHR^-$, and $Ru^{IV}{=}NR^{2-}$) have been electrochemically and spectroscopically characterized. Spectral assignments have been made with the aid of DFT computations. Such computations have also provided support for the existence of three other short-lived intermediates ($Ru^{V}{=}NR^{2-}$, $Ru^{II}-NOHR$, and $Ru^{II}-NHOHR$).

Acknowledgment. Acknowledgment is made to the Donors of the American Chemical Society Petroleum Research Fund for support of this research (Grant ACS PRF No. 40944-B3). We thank Professors Rodger Nutt and Durwin Striplin for their helpful discussions.

Supporting Information Available: Complete information for ref 14, ^1H NMR data for $[Ru^{II}(bpy)_2(mpea)](PF_6)_2$ and $[Ru^{II}(bpy)_2(mpeNO)](PF_6)_2$, description of the principal component analysis of the spectroelectrochemical data, information on the acidity of $Ru^{III}-NH_2R$, Mulliken population analysis, and b3lyp/cep-31g(d) geometries. This material is available free of charge via the Internet at http://pubs.acs.org.

IC800483G